Determination of Interfacial Debond Mode for Fiber-Reinforced Cementitious Composites

By Victor C. Li,[1] Member, ASCE, and Yin-Wen Chan[2]

Abstract: Theoretical models of mechanical properties of fiber reinforced cementitious composites require assumptions of fiber-cement interfacial behavior. In this paper, strength-based and fracture-based fiber debonding criteria are reviewed. To determine whether interfacial debonding is governed by the bond strength or critical energy release rate of the fiber-matrix interphase, fiber pull-out experiments were conducted using steel and brass wires of various diameters. The bond properties, including effective bond strength and frictional stress, were interpreted through a theoretical model of fiber pull-out. It was found that, for the material systems tested, interfacial debonding is dominated by frictional stress which is independent of the fiber diameters. Therefore, the debond mode of these material systems is categorized as strength-based. In general, the debond mode is a material characteristic and is dependent on the specific fiber and matrix types. In order to precisely predict the mechanical response of a fiber reinforced cementitious composite, it is necessary to determine the debond mode for a particular material system following the methodology proposed in this paper.

INTRODUCTION

The debonding behavior of fibers strongly affects the properties of fiber-reinforced composites. A reasonable composite model needs to be consistent with a realistic description of the debonding behavior of fibers. In the literature, two different approaches to the fiber debonding problem have been developed, namely strength-based and fracture-based approaches. In strength-based approaches (Lawrence 1972; Gopalaratnam and Shah 1987; Naaman et al. 1991; Leung and Li 1991), debonding is assumed to occur once an interfacial bond strength is reached. In fracture-based approaches (Stang and Shah 1986; Morrison et al. 1988; Gao et al. 1988; Leung 1992), the debonded interfacial zone is regarded as a tunnel crack which grows in length once an interfacial toughness is overcome at the crack tip.

There may exist a transition zone between the elastic bonded region and the frictional debonded region (Leung and Li 1990a). The debond mode of a particular material system is determined by the size of this transition zone, in comparison to fiber-embedment length, and the difference in stress distribution between the bonded and debonded regions of the interphase. In general, large transition zone and small difference between elastic bond strength and frictional stress will lead to a strength controlled debond mode. The transition zone size may be expected to depend on the microstructural size scale of the interphase. Thus cementitious composites with a relatively coarse microstructure is likely to have a larger transition zone than in fine-grain ceramic composites. It is suggested that the debond mode varies with the constituent material involved, such as fibers with different material type

[1]Prof., Advanced Civ. Engrg. Mat. Res. Lab., Dept. of Civ. and Envir. Engrg., Univ. of Michigan, Ann Arbor, MI 48109-2125.

[2]Grad. Res. Asst., Advanced Civ. Engrg. Mat. Res. Lab., Dept. of Civ. and Envir. Engrg., Univ. of Michigan, Ann Arbor, MI.

Note. Discussion open until September 1, 1994. To extend the closing date one month, a written request must be filed with the ASCE Manager of Journals. The manuscript for this paper was submitted for review and possible publication on February 19, 1993. This paper is part of the ***Journal of Engineering Mechanics***, Vol. 120, No. 4, April, 1994. ©ASCE, ISSN 0733-9399/94/0004-0707/$2.00 + $.25 per page. Paper No. 5659.

or surface treatments, cement matrix with various water/cement (w/c) ratios or additives, and so on. Erroneous assumption of the debond mode will lead to the accessment of interfacial properties that have no real physical meaning. Since fiber debonding and interfacial bond properties play a central role in micromechanical models of fiber reinforced composite materials, it is necessary to establish the appropriate debond mode for a given material system.

Due to the characteristics of fiber debonding and pull-out processes, two material parameters are usually adopted to describe the interfacial bond properties of a fiber reinforced composite, namely interphasal bond strength and frictional stress for strength-based approach; interphasal critical energy release rate and frictional stress for fracture-based approach. The material parameters may be interpreted from experimental results based on the theoretical analytic solution to the fiber pull-out problem assuming either debonding criterion. In general, there are similarities between the solutions by different approaches, namely the essential features of solutions are similar regardless of whether interfacial debonding is governed by strength or fracture properties. The similarity between the solutions from the two approaches makes it impossible to determine whether debonding is strength governed or fracture governed if interfacial bond properties is measured with a single type of specimen. Comparison between the solutions of the two different approaches indicates that one needs to measure interfacial bond properties with specimens of different fiber diameters or different fiber volume fractions. The parameter that governs the debonding behavior has to be the intrinsic material property and shall not vary with fiber diameters or fiber volume fraction. Therefore, this concept serves as a methodology to identify the appropriate debond mode of a particular material system.

In this paper, the conditions for the two different approaches are discussed and the result from an experimental program based on the addressed conditions is presented to demonstrate the appropriate approach for various material systems. In the experimental program, the bond properties of selected steel and brass fibers were measured experimentally with respect to various fiber sizes. Based on the concept previously stated, the appropriate debonding criterion can be determined. It is found that, for both steel and brass fiber, the debond mode is strength governed since the interfacial bond strength is found to be identical to the frictional stress and is independent of the fiber diameters.

COMPARISON OF THEORETICAL SOLUTIONS OF STRENGTH- AND FRACTURE-BASED APPROACHES

When a fiber-reinforced composite material is subjected to tensile load and undergoes fracture failure, the reinforcing fibers may undergo various stages of interaction with the matrix. First, when the external load is low, the fiber-matrix interphase remains well bonded. This is followed by a stage of partial debonding when the load increases and overcomes the critical interfacial bond properties. Resistance of the applied load comes partly from the elastic bond on the bonded segment of the fiber and partly from the frictional bond on the debonded segment of the fiber. When the entire embedment length is completely debonded, the fiber may start to be pulled out. At this final stage, the fiber stress is mainly resisted by the frictional stress between fiber and matrix.

For most models dealing with interfacial debonding, two parameters are

usually assumed to be responsible. For strength-based approach, an interfacial bond strength τ_s and a frictional stress τ_i are adopted to characterize the fiber-matrix interphase for well-bonded and debonded regions correspondingly. Fiber-matrix interphase starts to debond when τ_s is reached. In debonded regions τ_i becomes the active resistance. For fracture-based approach, on the other hand, an interfacial critical energy release rate Γ is used to characterize the well-bonded region instead of bond strength τ_s. In debonded region, frictional stress τ_i is assumed as in strength-based approach.

During interfacial debonding, the fiber stress-displacement ($\sigma_p - u$) relation, of a single fiber subjected to pull-out load σ_p has been derived by Leung and Li (1991) using strength-based interfacial debonding and employing an axial-symmetric shear-lag model

$$\frac{u}{d_f} = \frac{\tau_s}{E_f(1-\alpha)\rho^2} + \left[\sigma_p - \frac{2\tau_i}{(1-\alpha)d_f} L_f\right] \frac{L_f}{E_f d_f} \tag{1}$$

A similar model but using fracture-based debonding (Leung 1992) leads to

$$\frac{u}{d_f} = \frac{1}{E_f(1-\alpha)\rho^2}\left[\tau_i + \sqrt{\frac{2E_f\Gamma(1-\alpha)\rho^2}{d_f}}\right] + \left[\sigma_p - \frac{2\tau_i}{(1-\alpha)d_f} L_f\right] \frac{L_f}{E_f d_f} \tag{2}$$

R^* is the radius of a matrix cylinder containing the fiber within which the matrix is assumed to deform in shear only and all axial stress is localized on the cylinder rim at R^* (Budiansky et al. 1986). In practice, ρ can be related to the initial slope S of the ascending branch of a pull-out curve as derived in Appendix I.

Eqs. (1) and (2) would be identical if an effective bond strength τ_{eff} is adopted

$$\tau_{\text{eff}} = \begin{cases} \tau_s; & \text{[in (1), strength-based approach]} \quad (3a) \\ \tau_i + \sqrt{\dfrac{2E_f\Gamma(1-\alpha)\rho^2}{d_f}}; & \text{[in (2), fracture-based approach]} \quad (3b) \end{cases}$$

so that

$$\frac{u}{d_f} = \frac{\tau_{\text{eff}}}{E_f(1-\alpha)\rho^2} + \left[\sigma_p - \frac{2\tau_i}{(1-\alpha)d_f} L_f\right] \frac{L_f}{E_f d_f} \tag{4}$$

The resulting expression (4) can be used for both strength-based and fracture-based debonding, provided τ_{eff} is interpreted as in (3).

The similarity between the solutions from the strength-based and fracture-based approaches has also been suggested by Stang et al. (1990). For fracture based debonding

$$\tau_{\text{eff}} = \tau_i + \sqrt{\frac{2k\Gamma}{\pi d_f}} \tag{5}$$

where k = an interfacial shear stiffness in Stang's plane-strain shear-lag model and other notations are the same as in previous equations.

The similarity between the solutions from the two approaches makes it impossible to determine whether debonding is strength governed or fracture governed if interfacial bond properties is measured with a single type of specimen. However, the dependency of τ_{eff} on d_f for the fracture models [(3) and (5)] and the independency of τ_{eff} on d_f for the strength models suggest a simple approach for identifying the true mode of interfacial debonding. While both τ_s and Γ can be derived from a given set of fiber pull-out test result according to (1) and (2), only one of these two parameters has physical meaning. In general, material parameters (e.g., yield strength or fracture toughness) should not be affected by specimen geometry. For instance, the yield strength of aluminum determined with various specimen sizes should give a constant value. Likewise, if a fiber-matrix material system follows strength-based debonding criterion, the interfacial bond strength measurement, via single fiber pull-out test for instance, shall not be affected by the fiber sizes employed as long as the fibers of various diameters are made by the same material with the same surface treatment. On the other hand, for material systems following fracture-based debonding criterion, the interfacial critical energy release rate or fracture toughness would be the true material parameter with respect to interphasal debonding. In this case, the measured Γs have to be constant regardless of various fiber sizes. If one tries to interpret a bond strength for this material system, the obtained "bond strength" must vary with fiber diameters and shall be regarded as τ_{eff} instead. If the debonding is fracture-based, the relation between τ_{eff} and fiber sizes d_f should be the one given by (3*b*) or (5).

In other words, the results of fiber pull-out test can always be interpreted to give τ_{eff} and τ_i. For various fiber diameters, if the resulted τ_{eff}s are constant, the material system is strength-governed, and $\tau_s = \tau_{eff}$. Composite micromechanical models should be based on τ_s and/or τ_i. On the other hand, if the interpreted τ_{eff} are not constant but vary with d_f in a way consistent with (3*b*), fracture approach would apply for this material system. In this case, a material constant Γ should be utilized in composite micromechanical models. This interfacial critical energy release rate can be interpreted from (3*b*) once τ_{eff} (d_f) is experimentally determined.

The experimental program of this study is based on the concept described above. Single fiber pull-out tests were conducted for two material systems, steel fiber-cement matrix and brass fiber-cement matrix, with various fiber diameters. τ_{eff} and τ_i were then determined by the procedure to be described in the next section. Dependency of the resulting τ_{eff} on d_f was then examined in an attempt to identify the interfacial debond mode.

EXPERIMENTAL PROGRAM

Single Fiber Pull-Out Test

Fiber pull-out tests were conducted in the test program by pulling individual fibers out of cement matrix. The single fiber pull-out test setup is shown in Fig. 1. Basically, a fiber sample is partially embedding in the dog-bone-shaped specimen and partially protruding. A hydraulic grip subjected to a constant displacement rate is adopted to hold the fiber such that no slip between the grip and the fiber may occur. The pull-out load is obtained from the load cell through a data-acquisition system. The corresponding displacement of the fiber protruded end is recorded simultaneously. In practice, the displacement of the fiber protruded end is obtained by subtracting the elastic stretch of the fiber free length from the relative displacement between the matrix base and the hydraulic grip. This relative displacement is measured using a clip gage. The elastic stretch of the fiber free length between the matrix base and the hydraulic grip at any given load is calculated based on the initial fiber free length, fiber cross-sectional area, and fiber elastic modulus.

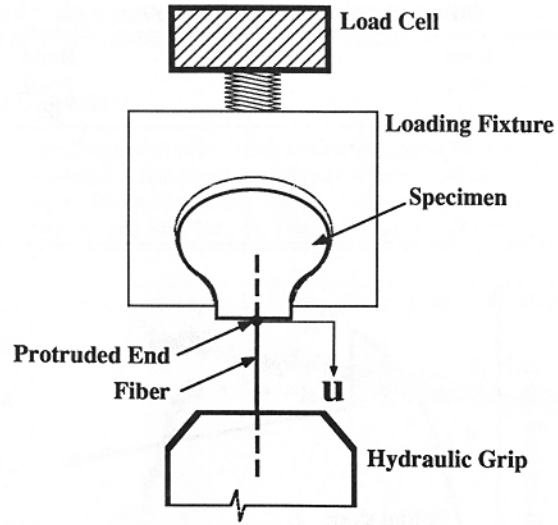

FIG. 1. Single Fiber Pull-Out Test Setup

TABLE 1. Compositions of Cement Matrix

(1)	Ingredient		
	Water/cement (w/c) (2)	SF/c[a] (%) (3)	SP/c[b] (%) (4)
Proportion	0.27	20	3

[a]Weight ratio of condensed silica fume to cement.
[b]Weight ratio of superplasticizer to cement.

Specimens were demolded 24 hr after casting and were cured in a water tank till testing. Fiber pull-out tests were conducted at three different ages (seven, 14, and 28 days) for steel-cement system and 28 days for brass-cement system; four diameters for steel wire and three diameters for brass wire were used. At least six specimens were tested for each case. Pull-out tests were conducted under a uniaxial hydraulic MTS testing machine.

Material Systems

The mix proportion of cement matrix is given in Table 1.

The fibers employed are steel and brass wires without any special surface treatment. Various fiber diameters are summarized in Table 2.

Different fiber-embedment lengths were used, namely 25 mm and 10 mm for steel and brass wires correspondingly. Unlike steel wires, brass wires have a much lower yield strength. To prevent brass wires from yielding due to high pull-out loads, it is decided to use a shorter embedment length for

TABLE 2. Diameters for Each Fiber Type

Steel (mm) (1)	Brass (mm) (2)
0.38	—
0.51	0.51
0.81	0.81
1.02	1.02

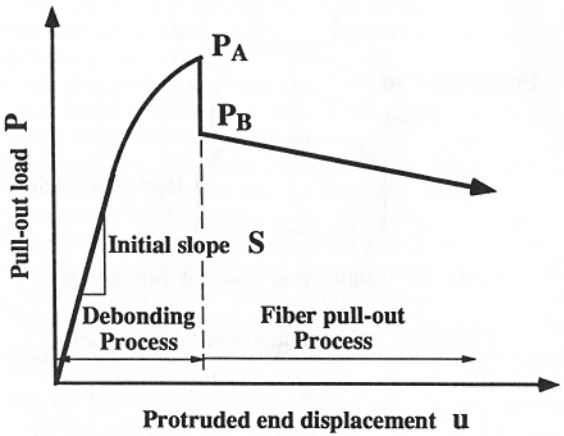

FIG. 2. Typical Pull-Out Curve

brass-cement system. Nevertheless, it has been experimentally verified (Chan and Li 1993) that the interfacial bond properties reported here are independent of the fiber-embedment lengths.

Interpretation of Test Results

During the fiber pull-out tests, the pull-out loads and the corresponding fiber slip distances of the protruded end, i.e., the P-u relation, were recorded. A typical P-u curve is given in Fig. 2. Several important features of a pull-out curve, including the peak load P_A, the load right after complete debonding P_B, and the slope of the linear portion of the ascending branch S are essential for interpretation of bond properties. Consequently, the effective bond strength τ_{eff} and the frictional stress τ_i are obtained by solving the following equations:

$$\tau_i = \frac{P_B}{\pi d_f L_f} \tag{6}$$

$$\sqrt{\left(\frac{\tau_{eff}}{\tau_i}\right)^2 - \left(\frac{\tau_{eff}}{\tau_i}\right)} - \cosh^{-1}\sqrt{\frac{\tau_{eff}}{\tau_i}} = \left(\frac{P_A}{P_B} - 1\right)\frac{L_f}{E_f}S \tag{7}$$

Derivation of (6) and (7) is given in Appendix I. In (6) and (7), E_f, L_f, and d_f are as defined previously, and S is the initial slope of P-u curves, Fig. 2, and is shown in Appendix I that $S = (2E_f\rho)/d_f$.

Consequently, the relation between the interpreted τ_{eff}s and the various fiber diameters d_f is examined to determine the debond mode based on (3).

RESULT AND COMMENT

Typical fiber pull-out curves, load P-displacement-u relation, are summarized in Figs. 3 and 4 for steel and brass wires, respectively. Generally, at each curing age, the pull-out curves of various fiber diameters for both steel and brass wires are similar. In Figs. 3 and 4, at the age of 28 days,

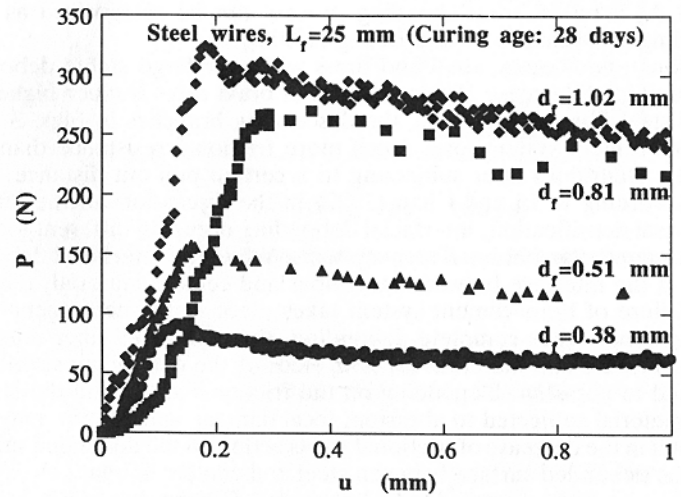

FIG. 3. Pull-Out Curves of Steel-Cement System for Various Fiber Diameters at Age of 28 Days

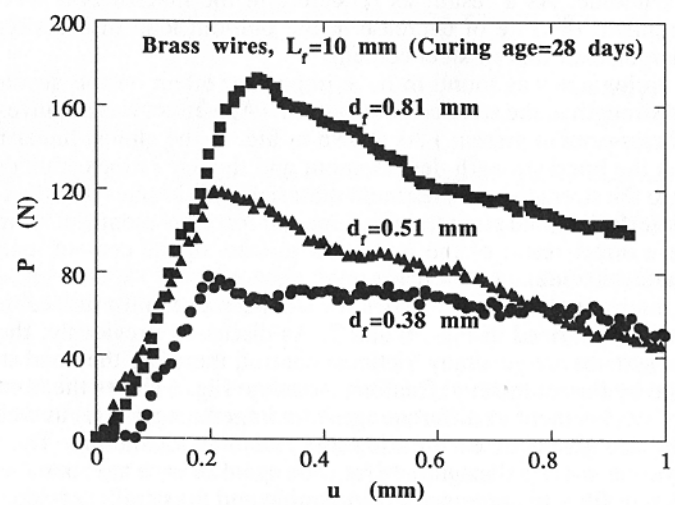

FIG. 4. Pull-Out Curves of Brass-Cement System for Various Fiber Diameters at Age of 28 Days

there is only a slight nonlinear portion before reaching the peak and the peak load is followed by a smooth descending branch. In other words, there is no load drop detected according to the specimens tested. As indicated previously, in typical pull-out process, there might be a load drop following the peak load as a result of unstable debonding. The difference between the peak load and the stationary load after the load drop, which refers to the total frictional resistance of the embedded portion, depends on the magnitude of τ_{eff} and τ_i. Based on the characteristics shown in Figs. 3 and 4, the current experimental results indicate that the steel and brass wires in the cement matrix used possess interfacial bond properties of identical τ_s and τ_i. As a result, the debonding process can be categorized as stable debonding according to Li and Leung (1991).

Although both cases, steel and brass wires, undergo stable debonding, the rate of load decrease after peak load of brass wires is much higher than that of steel fibers. Comparing the descending branches in Figs. 3 and 4, the brass-cement system loses much more frictional resistance than steel-cement system does after subjecting to a certain pull-out distance, say, 1 mm. According to Li and Chan (1992) in the discussion on the effect of interphasal densification, interfacial debonding occurs in different locations for steel-cement and brass-cement systems. While the interfacial debonding occurs at the interface between steel fiber and cement material, the interfacial failure of brass-cement system takes place in the heterogeneous interfacial zone. After complete debonding, the embedded fiber undergoes pull-out process and materials on both sides of the debonding surfaces are subjected to abrasion. Depending on the frictional stress and the strength of the material subjected to abrasion, local damage and rupture may occur and result in the decrease of frictional stress acting on the debonded surfaces. Since the debonded surface between steel and cement is relatively smooth, the abrasion may be expected to be less severe. For the case of brass-cement system, on the other hand, severe damage and fracture are expected to take place in the cement materials on the tortuous debonded surfaces of the interfacial zone. As a result, as reflecting in the macroscopic mechanical measurement, the rate of decrease in the pull-out load of brass-cement is much larger than that of steel-cement.

The curing age was found to have important effect on the development in bond strength in the steel-cement system. (Age effect was not investigated in the brass-cement system.) As shown in Fig. 5, the almost linear relation between the bond strength development and the age in logarithmic scale is similar to the strength gain of cement material. This implies that the increase in the interfacial bond strength of a fiber-reinforced cementitious composite may be a direct result of the hydration process of the cement material in the interfacial zone.

The interpreted bond properties for steel-cement and brass-cement systems are summarized in Figs. 6 and 7. As discussed previously, the tested material systems are generally frictional control, therefore the bond strengths are given by the interpreted frictional stresses. Fig. 6 shows the bond properties of steel-cement at different ages. Averaged magnitudes as well as the variation are given for each curing age and fiber diameters. The dashed lines show the averaged magnitude for each age. For each age, bond strengths for different fiber diameters are comparable and no significant dependency on fiber diameter can be found. According to the criteria of debond mode discussed previously, the interfacial debonding of steel-cement system may

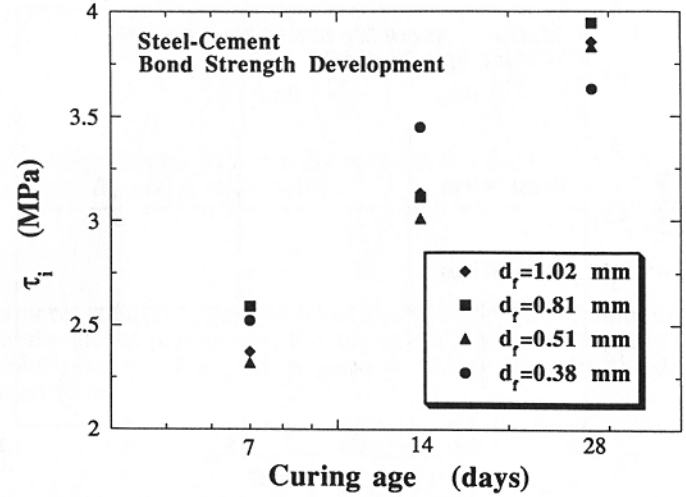

FIG. 5. Effect of Curing Age on Steel-Cement Bond Strength Development

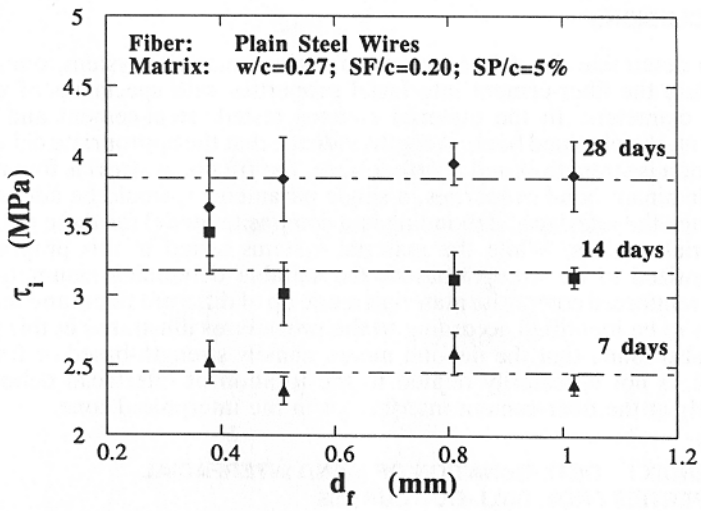

FIG. 6. Steel-Cement Bond Strength Determined from Pull-Out Test using Four Fibers with Different Diameters

therefore be identified as strength-based. Similarly, the brass-cement system (Fig. 7) also follows a strength-based debond mode.

Although interfacial debonding occurs in different locations, the fiber-matrix interface for steel-cement and the interphasal zone for brass-cement (Li and Chan 1992), the debond mode of the two material systems are both determined to be strength-based. This implies that the debond mode is not necessarily related to the location of debonding.

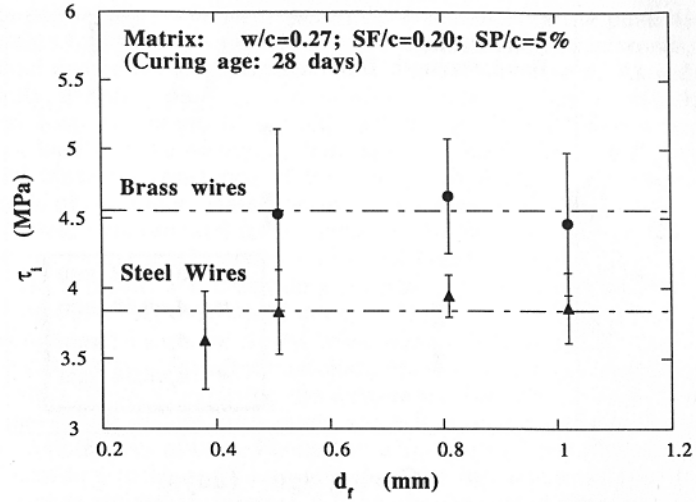

FIG. 7. Comparison of Bond Strength–Fiber Diameter Relation between Steel-Cement and Brass-Cement Systems

CONCLUSIONS

To determine the debond mode of a given material system, one has to measure the fiber-cement interfacial properties with specimens of various fiber diameters. In the material systems tested, steel-cement and brass-cement, the obtained bond strengths indicate that the appropriate debonding criterion is strength-based. Furthermore, the frictional stress is found to be the dominant bond properties, a single parameter τ_i would be adequate to describe the interfacial debonding in a composite model for these particular material systems. While the material systems tested in this program are categorized to be strength-based, the suitable debonding assumption for fiber reinforced composite materials made up of different fibers and matrices needs to be identified according to the procedures illustrated in this paper. It is also found that the debond mode, namely strength-based or fracture-based, is not necessarily related to the location of interfacial debonding, namely at the fiber-cement interface or in the interphasal zone.

APPENDIX I. DETERMINATION OF ρ AND INTERFACIAL PROPERTIES FROM PULL-OUT CURVES

Determination of ρ from Initial Slope S of $\sigma_p - u$ Curves

Although the parameter ρ appearing in (3) can be obtained in principle from V_f, E_f, E_m, G_m, etc., for convenience, it is decided to use the initial slope S of the $\sigma_p - u$ experimental curve.

According to Leung and Li (1990b), in the elastically bonded stage, the displacement at the protruded end is given by

$$u = \frac{\tau(0)}{G_m}\left[\frac{d_f}{2}\log\left(\frac{R^*}{r_f}\right)\right] \tag{8}$$

and the shear stress at the protruded end $\tau(0)$ is given by

$$\tau(0) = \frac{\rho}{2}\sigma_p\left[\frac{(1-\alpha)}{\tanh\left(\frac{2\rho L_f}{d_f}\right)} + \frac{\alpha}{\sinh\left(\frac{2\rho L_f}{d_f}\right)}\right] \tag{9}$$

For pull-out specimens, V_f is usually very small, i.e., $V_f \approx 0$.

Thus, $E_c \approx E_m$ and $\alpha \ll 1$, where

$$\alpha = \frac{E_f V_f}{E_c}$$

Furthermore, $\tanh[(2\rho L_f)/d_f] \approx 1$ when $(2\rho L_f)/d_f > 5$. This condition applies to general material parameters. For the material systems tested in this experimental program, $(2\rho L_f)/d_f$ is generally larger than 10 based on the expression for ρ

$$\rho^2 = \frac{2G_m E_c}{V_m E_m E_f \log\left(\frac{R^*}{r_f}\right)} \tag{10}$$

Thus, from (9)

$$\tau(0) \approx \frac{\rho}{2}\sigma_p$$

and

$$u = \sigma_p\left[\frac{\rho d_f}{4G_m}\log\left(\frac{R^*}{r_f}\right)\right] \tag{11}$$

Therefore, from (11) the initial slope S of $\sigma_p - u$ curves can be obtained

$$S = \left.\frac{\sigma_p}{u}\right|_{\text{at the protruded end}} = \frac{4G_m}{\rho d_f \log\left(\frac{R^*}{r_f}\right)} \tag{12a}$$

$$S \approx \frac{2}{d_f}\sqrt{\frac{2G_m E_f}{\log\left(\frac{R^*}{r_f}\right)}} \tag{12b}$$

where ρ has been substituted by

$$\sqrt{\frac{2G_m E_c}{V_m E_m E_f \log\left(\frac{R^*}{r_f}\right)}}$$

Therefore

$$\log\left(\frac{R^*}{r_f}\right) = \frac{8G_m E_f}{d_f^2 S^2} \tag{13}$$

Hence, by substituting (13) into (12), the parameter ρ can be determined from the initial slope S of $\sigma_p - u$ curves

$$\rho = \frac{d_f}{2E_f} S \tag{14}$$

Interpretation of τ_s and τ_i

It has been assumed that the applied load in the descending portion is mainly resisted by the friction between fiber and matrix. By equilibrium, we have

$$P_B = (\pi d_f L_f)\tau_i$$

Therefore

$$\tau_i = \frac{P_B}{\pi d_f L_f} \tag{15}$$

According to Leung and Li (1990b)

$$\frac{P_A}{P_B} = 1 + \frac{d_f}{2\rho L_f}\left[\sqrt{\left(\frac{\tau_s}{\tau_i}\right)^2 - \left(\frac{\tau_s}{\tau_i}\right)} - \cosh^{-1}\sqrt{\frac{\tau_s}{\tau_i}}\right]$$

Rewriting the preceding equation and substitute ρ in terms of S as given in (14)

$$\sqrt{\left(\frac{\tau_s}{\tau_i}\right)^2 - \left(\frac{\tau_s}{\tau_i}\right)} - \cosh^{-1}\sqrt{\frac{\tau_s}{\tau_i}} = \left(\frac{P_A}{P_B} - 1\right)\frac{L_f}{E_f} S \tag{16}$$

Therefore, τ_s/τ_i can be determined in terms of P_A/P_B and S. With the considerations leading to (3), τ_s in (16) can be replaced by τ_{eff}, resulting in (7).

For a special case, where no load drop occurs when the fiber is completely debonded as mentioned previously, $P_A = P_B$. This will result in a solution of $\tau_s/\tau_i = 1$, which is the condition for stable debonding.

ACKNOWLEDGMENT

The authors acknowledge the support of portions of this work by a grant from the National Science Foundatdion (Grant No. BCS 9202097) to the University of Michigan.

APPENDIX II. REFERENCES

Budiansky, B., Hutchinson, J. W., and Evans, A. G. (1986). "Matrix fracture in fiber-reinforced ceramics." *J. Mech. Phys. Solids*, 34(2), 167–189.

Chan, Y. W., and Li, V. C. (1993). "Interfacial debond mode of steel fibers in cement matrix." *ACI special publication*, American Concrete Institute (ACI), Detroit, Mich.

Gao, Y., Mai, Y. W., and Cotterell, B. (1988). "Fracture of fiber-reinforced materials." *J. Appl. Math. and Phys. (ZAMP)*, 39, 550–572.

Gopalaratnam, V. S., and Shah, S. P. (1987). "Tensile fracture of steel fiber reinforced concrete." *J. Engrg. Mech.*, ASCE, 113(5), 635–653.

Lawrence, P. (1972). "Some theoretical considerations of fiber pull-out from an elastic matrix." *J. Mat. Sci.*, 7(1), 1–6.

Leung, C. K. Y. (1992). "A fracture-based two-way debonding model for discontinuous fibers in an elastic matrix." *J. Engrg. Mech.*, 118(11), 2298–2318.

Leung, C. K. Y., and Li, V. C. (1990a). "Strength-based and fracture-based approaches in the analysis of fiber debonding." *J. Mat. Sci. Letters*, 9, 1140–1142.

Leung, C. K. Y., and Li, V. C. (1990b). "Applications of a two-way debonding theory to short-fiber composites." *Comp.*, 21(4), 305–317.

Leung, C. K. Y., and Li, V. C. (1991). "A new strength based model for the debonding of discontinuous fibers in an elastic matrix." *J. Mat. Sci.*, 26, 5996–6010.

Li, V. C., and Chan, Y. W. (1992). "Effect of interphase densification on the microstructure and bond strength of a steel fiber reinforced cementitious composite." *J. Am. Ceram. Soc.*

Li, V. C., and Leung, C. K. Y. (1991). "Tensile failure modes of random discontinuous fiber reinforced brittle matrix composites." *Fracture processes in concrete, rock and ceramics*. Chapman and Hall, London, England, 285–294.

Morrison, J. K., Shah, S. P., and Jenq, Y. S. (1988). "Analysis of fiber debonding and pullout in composites." *J. Engrg. Mech.*, 114(2), 277–294.

Naaman, A. E., Namur, G. C., Alwan, J. M., and Najm, H. (1991). "Fiber pullout and bond slip. I: analytical study." *J.Engrg. Mech.*, ASCE, 117(9), 2769–2790.

Stang, H., Li, Z., and Shah, S. P. (1990). "The pull-out problem—the stress versus fracture mechanical approach." *J. Engrg. Mech.*, ASCE, 116(10), 2136–2150.

Stang, H., and Shah, S. P. (1986). "Failure of fiber reinforced composites by pull-out mechanical approach." *J. Engrg. Mech.*, ASCE, 21(3), 953–958.

APPENDIX III. NOTATIONS

The following symbols are used in this paper:

d_f = fiber diameter;
E_c = modulus of elasticity of composite;
E_f = modulus of elasticity of fiber;
E_m = modulus of elasticity of matrix;
G_m = matrix shear modulus;
L_f = fiber-embedment length;
P = fiber pull-out load;
P_A = peak load of P-u curve;
P_B = load right after complete debonding;
R^* = radius of matrix cylinder containing fiber within which matrix is assumed to deform in shear only;
r_f = fiber radius;
S = initial slope of P-u curve;
u = displacement of the protruded end of fiber;
V_f = fiber volume fraction;
V_m = matrix volume fraction;
α = $(E_f V_f)/E_c$;
Γ = interfacial critical energy release rate;
ρ^2 = $(2G_m E_c)/[V_m E_m E_f \log(R^*/r_f)]$;
σ_p = fiber stress at protruded end;
τ_i = fiber-matrix frictional stress; and
τ_s = interfacial bond strength.